J Physiol 587.20 (2009) pp 4873–4886

The Journal of Physiology

Myostatin represses physiological hypertrophy of the heart and excitation–contraction coupling

Buel D. Rodgers[1,2], Jillian P. Interlichia[1], Dilip K. Garikipati[2], Ranganath Mamidi[3], Murali Chandra[3], O. Lynne Nelson[4], Charles E. Murry[5] and Luis F. Santana[6]

[1]*Department of Animal Sciences,* [2]*School of Molecular Biosciences,* [3]*Department of Veterinary Comparative Anatomy, Pharmacology & Physiology and* [4]*Department of Veterinary Clinical Sciences, Washington State University, Pullman, WA 99164, USA*

[5]*Center for Regeneration Medicine, Department of Pathology and* [6]*Department of Physiology & Biophysics, University of Washington, Seattle, WA 98195, USA*

Although myostatin negatively regulates skeletal muscle growth, its function in heart is virtually unknown. Herein we demonstrate that it inhibits basal and IGF-stimulated proliferation and differentiation and also modulates cardiac excitation–contraction (EC) coupling. Loss of myostatin induced eccentric hypertrophy and enhanced cardiac responsiveness to β-adrenergic stimulation *in vivo*. This was due to myostatin null ventricular myocytes having larger $[Ca^{2+}]_i$ transients and contractions and responding more strongly to β-adrenergic stimulation than wild-type cells. Enhanced cardiac output and β-adrenergic responsiveness of myostatin null mice was therefore due to increased SR Ca^{2+} release during EC coupling and to physiological hypertrophy, but not to enhanced myofilament function as determined by simultaneous measurement of force and ATPase activity. Our studies support the novel concept that myostatin is a repressor of physiological cardiac muscle growth and function. Thus, the controlled inhibition of myostatin action could potentially help repair damaged cardiac muscle by inducing physiological hypertrophy.

(Received 17 March 2009; accepted after revision 1 September 2009; first published online 7 September 2009)
Corresponding author B. D. Rodgers: Department of Animal Sciences and School of Molecular Biosciences, Washington State University, Pullman, WA 99164, USA. Email: danrodgers@wsu.edu

Abbreviations Acvr2 and Acvr2b, a.k.a. ActRIIa and ActRIIb, activin type II receptors; ALK, activin-like kinase; ANP, atrial natriuretic peptide; BNP, B-type natriuretic peptide; CS, cell shortening; Cdk, cyclin-dependent kinase; EF, ejection fraction; ET, ejection time; ENT, equilibrative nucleoside transporter; EC, excitation–contraction; FSTL, follistatin-like; FS, fractional shortening; GASP, growth factor associated serum protein; HR, heart rate; IGF, insulin-like growth factor; IGFBP, IGF binding protein; IVS, intraventricular septum; ISO, isoproterenol; IVRT, isovolumic relaxation time; LVID, left ventricle internal diameter; LVW, LV wall dimension; MHC, β-myosin heavy chain; ODU, optical density unit; SR, sarcoplasmic reticulum; TGF, transforming growth factor; VDCC, voltage dependent calcium channel.

Introduction

Myostatin is a potent negative regulator of skeletal muscle growth and a member of the transforming growth factor (TGF)-β superfamily (Rodgers & Garikipati, 2008). The myostatin null phenotype is associated with hypermuscularity and is often referred to as 'double muscling'. Its actions are mediated by the activin type II receptors Acvr2 and Acvr2b (a.k.a. ActRIIa and ActRIIb) and by the type I receptors activin-like kinase (ALK)4 and ALK5. They can also be manipulated by follistatin, follistatin-like (FSTL)-3 and by growth/differentiation factor associated serum protein (GASP)-1, as these proteins are all capable of binding myostatin and attenuating receptor activation. Although primarily expressed and initially characterized in mammalian skeletal muscle, myostatin expression has been reported in a number of fish tissues (Garikipati *et al.* 2006, 2007; Helterline *et al.* 2007), which led to its detection in a few other mammalian tissues, including the heart. The functional significance of myostatin expression and bioactivity in cardiac muscle, however, has not been determined.

Myostatin is expressed in both fetal and adult ovine hearts, specifically in the cardiomyocytes and Purkinje fibres (Sharma *et al.* 1999; Shyu *et al.* 2005), and is co-expressed with FSTL-3 and follistatin in the ventricles, atria and/or valves of developing mice and chicken

DOI: 10.1113/jphysiol.2009.172544

(Takehara-Kasamatsu *et al.* 2007; van den Berg *et al.* 2007). Its expression also similarly increases with insult in both cardiac and skeletal muscle (Rodgers & Garikipati, 2008), suggesting that myostatin may additionally influence the growth and development of both tissues. The myokine is differentially expressed in cardiomyocytes during cardiac development and high levels of expression are correlated with a low proliferation index (McKoy *et al.* 2007). Recent studies have in fact raised the intriguing possibility that myostatin may indeed influence cardiac muscle growth and suggest that it may function as a chalone in both skeletal and cardiac muscle (Cook *et al.* 2002; Gaussin & Depre, 2005; Shyu *et al.* 2005). Whether myostatin has the ability to regulate cardiac muscle development and function remains unknown, however.

Herein we report myostatin's inhibitory effects on different cardiomyoblast growth processes as well as the functional assessment of cardiac performance in myostatin null mice and primary ventricular myocytes. These studies suggest that myostatin suppresses basal and IGF-stimulated proliferation as well as cellular differentiation; actions that are conserved in skeletal muscle cells. Echocardiography indicates that stress-induced cardiac performance is enhanced in myostatin null mice, which also have enlarged hearts, while Ca^{2+} handling and contractility is similarly enhanced in their primary cardiomyocytes. The myostatin null mouse, therefore, appears to be a novel and unexplored model of cardiac hypertrophy that strongly resembles physiological, but not pathological states.

Methods

Ethical approval

These studies were pre-approved by an interdepartmental dissertation committee and by two separate Institutional Animal Care and Use Committees at Washington State University and the University of Washington in accordance with the National Institutes of Health's *Guide for the Care and Use of Laboratory Animals*. A total of 199 mice (183 adults and 16 neonates) and 1 rat were used in these studies. All animals were killed and anaesthetics and analgesics were used according to the approved protocols as briefly described below.

Proliferation and differentiation assays

Rat H9C2 cardiomyoblasts (ATCC, www.atcc.org) were cultured at 37°C in a 5% CO_2 humidified atmosphere in Dulbecco's modified Eagle's medium (DMEM) (Sigma, www.sigmaldrich.com) supplemented with 10% fetal bovine serum (FBS), 0.2 mM glutamine, 100 IU ml^{-1} penicillin, 0.1 mg ml^{-1} streptomycin and 250 ng ml^{-1} amphothericin B. Proliferation assays were performed on cells originally plated at 50% confluency and in serum-free DMEM supplemented with 2.7, 11 or 55 nM long R3 (LR3) IGF-I (Diagnostic Systems Laboratories, www.dslabs.com) for 24 and 48 h. Cells were also cultured with 2.7 nM LR3 with 0, 2.7 nM or 11 nM human myostatin (MetaMorphix, www.metamorphixinc.com) for 48 h of incubation and total cell number was measured using the Cell Titer 96 proliferation assay (Promega, www.promega.com). To differentiate, cells were grown to 70% confluency in DMEM supplemented with 1% FBS and stimulated with 10 nM retinoic acid (Sigma) daily as described (Menard *et al.* 1999). To determine myostatin's effect on differentiation, cells were differentiated for 3–6 days with or without 11 nM myostatin. Myostatin was added at the beginning of the experiment and on day 3 in the 6-day group. Quantitative RT-PCR was performed to measure the expression of equilibrative nucleoside transporter (ENT)-1 at both time points and semi-quantitative RT-PCR to measure the expression and ratios of skeletal (α_{1s}) and cardiac (α_{1c}) L-type voltage-dependent calcium channels (VDCCs) at day 3 as both are markers of H9C2 differentiation into a cardiac phenotype (Menard *et al.* 1999; Leung *et al.* 2007).

Animals

Rat tissue samples were obtained from animals bred at the experimental animal laboratory building, Washington State University. Myostatin null mice were generously donated by Prof. Se-Jin Lee, Johns Hopkins University, and were maintained in the same facility. Mice used in the infarction studies were housed in facilities at the University of Washington and in each case, animals were housed in environmentally controlled rooms with 12 h daily light.

Myocardial infarctions were induced in wild-type mice using the ischaemia–reperfusion model as described (Robey & Murry, 2008). Briefly, mice were anaesthetized by injecting intraperitoneally a cocktail of 60 $\mu g\,g^{-1}$ ketamine, 50 $\mu g\,g^{-1}$ pentobarbital and 0.2 U g^{-1} heparin. Ophthalmic ointment was applied to the eyes and mice were placed on a 38°C water blanket, intubated and attached to a ventilator. A left thoracotomy was performed through the fifth intercostal space, the chest was exposed with a retractor and the pericardium was incised. Ischaemia was achieved by tying a suture around a sterile polyethylene tube that was placed on top of the proximal left anterior descending artery for 30 min. Successful ischaemia distal to the ligation site was verified visually while reperfusion was achieved by removing the tubing and suture. Chests were then closed in layers, saline and a buprenorphine bolus (0.05 mg kg^{-1}) were administered subcutaneously and mice were allowed to recover with hydrating gel and food placed directly into

Table 1. Primer sequences and annealing temperatures

Gene product	Forward/reverse primer sequences (5′ – 3′)	°C
Acvr2a	TGGCGTTCGCCGTCTTTCTTATC/AGTGTGGACAGATGGTGCAAC	60
Acvr2b	CAGGTTGGCACCAGACGGTAC/TCGATGGTCACGCAGAGCTGG	55
ALK-4	TGCCCAGTGGACACCTCAAGG/TGGACTCCTCCAGAATTGCACCTC	60
ALK-5	CCGAGACAGGCCATTTGTTTGT/TCGTGGATTCCGCCAATGGAAC	60
follistatin	GCGGGCTCTGCCTCCTGCTG/TTCCACCACCGCACTGGATGTC	70
FSTL-3	TCTGCTGGTACTTTGGGGCCAC/AGCCTGGTCCAACTTCACCCA	65
GASP-1	GCTCCCCTTCGAGGCCTAGC/GTCCTCACTGTCTGGGGGCTTCAG	63
MSTN	GCTGATTGCTGCTGGCCCAGTGG/GAGCACCCACAGCGGTCTACTACC	60
β-actin	CGCTGCGCTGGTCGTCGACAACG/ATCGTACTCCTGCTTGCTGATCCAC	60
ENT-1	TCATGCGAAAGCACCGAG/GGCACAGATCATGGCAAC	57
Myf-5	TGTATCCCCTCACCAGAGGAT/GGCTGTAATAGTTCTCCACCTGTT	55
EF-2	GACATCACCAAGGGTGTGCAG/GCAGTCAGCACACTGGCATA	62
BAMBI	TGTCCTCTCTCCTCCCAAGA/TGTCCATGGAAGCTGTAGTG	60
MSTN-qPCR	GGCCATGATCTTGCTGTAAC/TTGGGTGCGATAATCCAGTC	59
follistatin-qPCR	AATGCCTACTGTGTGACCTGT/GGCTCATCCGACTTACTGT	59
FSTL-3-qPCR	TGGTCTGGACAGTGGGATCCGT/TCCCGGCTGACACGAGTCTT	59
GAPDH-qPCR	GACCCCTTCATTGACCTCAAC/GATGACCTTGCCCACAGCCTT	59

the bedding. After 28 days, mice were anaesthetized as above, hearts were excised and non-infarcted, border zone (peri-infarcted) and infarcted tissue were dissected and snap frozen.

Qualitative and quantitative RT-PCR

Total RNA was extracted from cells, cardiac muscle and skeletal muscle using Trizol reagent (Invitrogen, www.invitrogen.com). Tissues were first snap frozen in liquid nitrogen, pulverized while frozen and homogenized in Trizol. RNA was treated with DNase (DNase RQ-1, Promega) and its integrity was assessed by agarose gel electrophoresis. Reverse transcription was performed on 1 μg RNA from infarcted mouse tissue and 5 μg RNA from rat tissue and cells using the First Strand cDNA synthesis kit (Invitrogen). In all assays, template loading was controlled by adding an equal volume of cDNA to a master mix for each sample, which was then aliquoted before the addition of gene-specific primers.

Primers and the annealing temperatures used in the qualitative RT-PCR assays for Acvr2, Acvr2b, ALK-4, ALK-5, follistatin, FSTL-3, GASP-1, ENT-1, bone morphogenic protein/activin membrane-bound inhibitor (BAMBI) and β-actin are included in Table 1. The PCR protocol included an initial denaturation of 94°C for 1 min, followed by 30, 35 or 40 cycles of 94°C for 30 s, a gene-specific annealing temperature for 30 s and 72°C for 90 s. Relative, but not absolute, differences in expression levels were reliably estimated as no differences in the expression of the loading control, β-actin, was observed.

Quantitative RT-PCR assays were conducted using the iCycler iQ Real-time PCR Detection System (Bio-Rad, www.bio-rad.com) and gene specific primers for ENT-1 and elongation factor (EF)-2 (Table 1). To determine myostatin's effect on H9C2 cell differentiation, cDNA was amplified at 95°C for 10 s, followed by 57°C for 30 s and 72°C for 30 s using primer concentrations that were empirically determined (ENT-1 FP = 400 nM, ENT-1 RP = 200 nM; EF-2 FP = 200 nM, RP = 200 nM). Melt curve analysis was performed with each primer set to assure specificity. In addition, amplicons were isolated on a 1% agarose gel to check for genomic DNA contamination or non-specific amplification. A master mix containing iQ Super mix (Bio-Rad) was aliquoted before addition of cDNA and these samples were subsequently divided in half before primers were added. Samples were run in triplicate and each analysis was duplicated. Relative gene expression of ENT-1 was, therefore, normalized to that of the EF-2 using the Q-Gene method (Muller *et al.* 2002). Similar assays were performed on mouse heart cDNA using gene specific primers for myostatin (Shao *et al.* 2007), follistatin (Farnworth *et al.* 2006), GAPDH (Drummond *et al.* 2002) and FSTL-3 (Table 1). The samples were amplified at 94°C for 30 s, followed by 59°C for 30 s and 72°C for 30 s using primer concentrations that were empirically determined (myostatin FP = 900 nM, RP = 900 nM; follistatin FP = 600 nM, RP = 900 nM; GAPDH FP = 900 nM, RP = 900 nM; FSTL-3 FP = 600, RP = 900). Levels and ratios of α1s and α1c VDCC expression were determined using semi-quantitative RT-PCR as described by Menard *et al.* (1999) after first determining the linear portion of the amplification curve for both gene products. Amplicon levels were measured optically on a gel and normalized to the optical density units (ODUs) of β-actin, and expressed as a percentage.

Assessment of cardiac function and mass

Male and female mice (3 each) were anaesthetized in a closed system chamber with 2.5% isoflurane in oxygen and maintained for the duration of the procedure with a nasal cone delivering 1% isoflurane. Standard imaging planes, M-mode, Doppler and functional calculations were obtained according to American Society of Echocardiography guidelines using the Acuson C512 echocardiography system (Siemens Medical Solutions, www.medical.siemens.com) with a model 15L8 15 MHz epicardial transducer. The LV parasternal long axis four-chamber view was used to derive ejection fraction (%EF) as well as ventricular dimensions and volumes. The left parasternal short axis view was used to obtain M-mode ventricular wall measures. The subcostal long axis view from the left apex was used for Doppler imaging of mitral inflow and aortic ejection profiles. After obtaining baseline echocardiograms for each mouse, stress tests were performed by injecting 10 mg kg^{-1} isoproterenol (ISO; Isuprel-R, Abbott Laboratories, www.abbott.com) intraperitoneally. Echocardiograph measurements were then recollected 3 min after injection. To independently validate estimates of heart mass, neonatal (<1 d.o.) and 7-month-old mice were anaesthetized using the ketamine/pentobarbital solution described above and hearts were removed and individually weighed.

$[Ca^{2+}]_i$ transients and contractility

Changes in $[Ca^{2+}]_i$ were determined using a membrane permeant acetoxymethyl-ester form of the fluorescent Ca^{2+} indicator Fluo-4 AM (Invitrogen) as previously described (Santana *et al.* 2002). Confocal imaging of whole-cell $[Ca^{2+}]_i$ transients was performed using a Bio-Rad Radiance 2000 confocal system coupled to a Nikon TE300 inverted microscope equipped with a Nikon 60× oil immersion lens (NA = 1.4). $[Ca^{2+}]_i$ images and cell edge detection were analysed with custom software written in the IDL language (ITT Visual Information Solutions, www.ittvis.com). The amplitude of the $[Ca^{2+}]_i$ transient evoked by the application of a Ca^{2+}- and Na^+-free (replaced with *N*-methyl-D-glucamine) solution was measured by adding 20 mM caffeine, although to ensure steady-state SR Ca^{2+} load, cells were subjected to a minimum of 10 preconditioning pulses (1 Hz) before caffeine was applied.

Simultaneous measurement of steady-state isometric force and MgATPase activity

Mice were anaesthetized with ketamine/pentobarbital as above and hearts were rapidly excised and placed into ice-cold high relaxing (HR) solution (mM: 20 2,3-butanedione 2-monoxime (BDM), 50 Bes, 20 EGTA, 6.29 $MgCl_2$, 6.05 Na_2ATP, 30 potassium propionate, 10 NaN_3, pH 7.0). A cocktail with the following protease inhibitors and 1 mM DTT was then added (final concentrations indicated): 4 mM benzamidine-HCl, 5 μM bestatin, 2 μM E-64, 10 μM leupeptin, 1 μM pepstatin and 200 μM PMSF. Papillary muscle bundles were carefully separated and removed from the left ventricle walls and thin fibre bundles (~150 μm × 1.5–2.0 mm) were dissected and skinned overnight in HR + 1% Triton X-100 (Chandra *et al.* 2006). Skinned fibres were then attached to a displacement motor (model 308B, Aurora Scientific, www.aurorascientific.com) and a force transducer (AE 801, Sensor One Technologies, www.sensorone.com) using aluminum T-clips. Sarcomere length was adjusted to 2.2 μm using a He–Ne laser diffraction system and readjusted to 2.2 μm after two full activation/relaxation cycles (de Tombe & Stienen, 1995). Fibres were immersed in 15 μl activating solutions with varying pCa (negative log of molar free Ca^{2+}, maximum = 4.3) and the following (in mM): 31 potassium propionate, 5.95 Na_2ATP, 6.61 $MgCl_2$, 10 EGTA, 10.11 $CaCl_2$, 50 Bes (pH 7.0), 10 NaN_3, 0.9 NADH, 10 phosphoenolpyruvate, pyruvate kinase (2000 U ml^{-1}), lactate dehydrogenase (208 U ml^{-1}), A_2P_5 (20 μM) and protease inhibitors. Isometric force and ATPase activity at 20°C were then measured simultaneously as described (de Tombe & Stienen, 1995; Chandra *et al.* 2001). Force developed at steady state was recorded on a chart recorder and sampled via an analog-to-digital converter. ATPase activity, as a function of pyruvate to lactate conversion and NADH breakdown, was measured by projecting near UV light through the muscle chamber and a beam splitter (50/50; 340 nm absorbance for changes in NADH concentration and 410 nm as a reference).

Statistical analysis

Three independent experiments were performed for the proliferation assays and two for the differentiation assays. Experiments performed on primary ventricular myocytes or on skinned fibres used multiple cells (see figure legends) isolated from at least four different animals per genotype. Differences between means were determined by a 1- or 2-way analysis of variance coupled to Fisher's *post hoc* least signifcant difference (PLSD) test or by Student's *t* test when appropriate ($P \leq 0.05$).

Results

Expression of myostatin, its binding proteins and its receptors

The H9C2 cell line was clonally derived from embryonic rat hearts and, when differentiated in the presence

of retinoic acid, adopts a cardiac muscle, not skeletal muscle, phenotype (Menard *et al.* 1999). We nevertheless confirmed the cardiac phenotype with a qualitative gene expression analysis of adult rat skeletal and cardiac muscle, proliferating H9C2 and L6 cells and of cells differentiating for 3 or 6 days (Fig. 1). Expression of ENT-1 and Myf-5 was used as differentiation and tissue-specific markers for cardiac and skeletal muscle, respectively, and changed as expected with differentiation. Myostatin expression was detected in proliferating H9C2 cells, but not in L6 cells (even after 40 cycles – data not shown), and decreased with differentiation. Expression of the different myostatin binding proteins also differed in the H9C2 and L6 cells, which was consistent with the differences in cardiac and skeletal muscle expression. Follistatin expression was higher in L6 cells, increased with differentiation and was similar in adult cardiac and skeletal muscle. By contrast, significant expression of FSTL-3 only occurred in cardiac tissue and decreased in differentiating H9C2 cells while GASP-1 expression was only detected in mature skeletal muscle.

Expression of the different receptors was similar in both cell types, with the exception of Acvr2 expression as it increased in differentiating L6 cells, but not in H9C2 cells. Its expression was also detected five cycles earlier than that of Acvr2b. The lengths, calculated annealing temperatures and GC content of the primers used to amplify Acvr2 and Acvr2b message were identical. Therefore, the difference is likely not to be due to primer efficiencies, but to differences in mRNA levels. Similarly, expression levels of ALK-5 were also higher than those of ALK-4.

Myostatin inhibits H9C2 cardiomyoblast proliferation and differentiation

H9C2 cells express all the important receptors necessary for myostatin signalling. Therefore, we determined if myostatin inhibits cardiomyoblast proliferation. Exogenous addition of myostatin significantly ($P \leq 0.05$) inhibited basal proliferation of H9C2 cells in a dose-dependent manner when cells were cultured in serum free medium for 48 h (Fig. 2*B*). Cell growth was inhibited by 8% and 21% with 11 and 22 nM myostatin, respectively, although the smaller dose of myostatin, 2.7 nM, did not have a significant effect.

IGF-I is a potent regulator of skeletal muscle growth and a determinant of animal size. It also stimulates proliferation of skeletal muscle cells (Adams, 2002). Addition of IGF-I stimulated the proliferation of H9C2 cells at 24 h and 48 h (Fig. 2*A*). This proliferative effect was only observed in serum free medium, but was dose dependent with a minimum dose of 2.7 nM significantly increasing total cell number. It has been reported that IGF binding proteins mediate the actions of myostatin in porcine myogenic cells (Kamanga-Sollo *et al.* 2003, 2005; Pampusch *et al.* 2005; Xi *et al.* 2005). Therefore, we examined whether myostatin inhibits the actions of IGF-I or LR3, an IGF-I analogue that does not bind IGF binding proteins (IGFBP), on cardiomyoblast proliferation. Myostatin significantly ($P \leq 0.05$) suppressed the stimulatory effect of both IGF-I and LR3 and in a similar manner (Fig. 2*C*). The suppressive effects were dose dependent as IGF-I-stimulated growth was inhibited by 14 and 23% with 2.7 and 11 nM myostatin, respectively. Myostatin had similar effects on LR3-stimulated proliferation (13 and 20%) suggesting that IGFBP sequestration of IGF-I is not involved.

Myostatin inhibits the differentiation of skeletal muscle cells by suppressing MyoD activity (Langley *et al.* 2002). Therefore, we examined myostatin's effect on the differentiation of cardiomyoblasts using quantitative

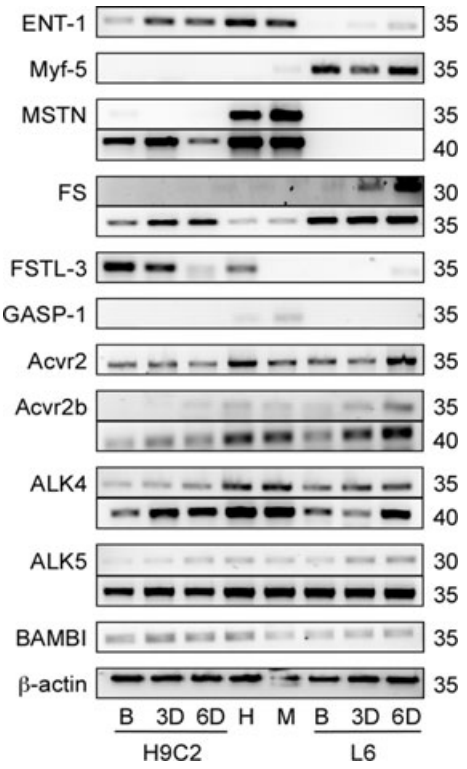

Figure 1. Qualitative expression of myostatin, its binding proteins and its receptors during differentiation
Equilibrative nucleoside transporter (ENT)-1 and myogenic factor (Myf)-5 were used as differentiation markers and β-actin as a loading control. Transcripts for myostatin (MSTN), follistatin (FS), follistatin-like (FSTL)-3, growth and differentiation factor associated protein (GASP)-1, activin type II receptors (Acvr2 and Acvr2b), activin like kinase (ALK4 and ALK5) and BMP and activin membrane-bound inhibitor (BAMBI) were amplified using qualitative RT-PCR. (B, myoblasts; 3D and 6D, days in differentiation medium; H, adult rat heart; M, adult rat skeletal muscle (gastrocnemius); H9C2, cardiomyoblasts; L6, skeletal myoblasts.) Samples were amplified for different numbers of cycles (right) to assure that comparisons are made within the linear phase of the amplification curve.

expression of ENT-1 as a marker. The levels of ENT-1 mRNA increased more than 3-fold after 3 days in differentiation medium, as expected (Leung *et al.* 2007), and remained constant thereafter (Fig. 2*D*). However, the addition of 11 nM MSTN partially suppressed ($P \leq 0.05$) the rise in ENT expression. It also prevented the differentiation-induced increase in α_{1c} VDCC expression, which is cardiac specific, after 3 days ($97 \pm 18\%$ β-actin ODUs w/o myostatin *vs.* $40 \pm 4\%$ w/myostatin, $P \leq 0.05$), but did not affect skeletal α_{1s} expression as it remained low in both groups. The suppressive effect on ENT-1 expression was not observed after 6 days in differentiation medium. Nevertheless, myostatin appears to inhibit the differentiation of this cardiac cell line in a manner similar to skeletal muscle cells.

Myostatin influence on cardiac performance and mass

To investigate the effect myostatin has on cardiac performance, echocardiography was performed on resting myostatin null and wild-type mice (Table 2 and Fig. 3). Left ventricular mass was significantly larger in the null mice as were the left ventricle internal diameters and volumes at diastole and systole (LVIDd, LVIDs, Diast. vol, Syst. vol), although intraventricular septum (IVSd) and (IVWd) wall diameters were similar in both groups. This indicates that the increased heart size in myostatin null mice is due to eccentric, not concentric, hypertrophy. Both heart and body weights of wild-type neonates were approximately 20% ($P \leq 0.05$) larger than those of myostatin null mice, although the heart weight to body weight (HW/BW) ratios were comparable in both groups (online Supplemental Material, Fig. S1). By contrast, adult hearts from the 7-month-old null mice used for echocardiography were almost 33% ($P \leq 0.05$) heavier than those from wild-type mice, which was similar to the differences in body weights (Fig. S1). In fact, the HW/BW ratios were nearly identical in both groups, suggesting that similar mechanisms may be responsible for both phenotypes. Measurements of heart weights from mice of various ages indicate that myostatin

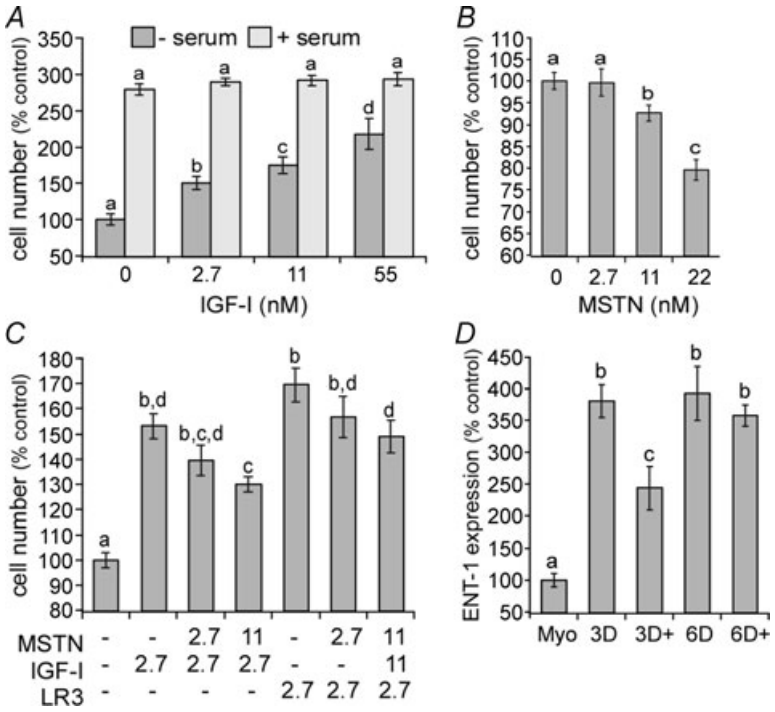

Figure 2. Myostatin inhibits IGF-stimulated and basal cardiomyoblast proliferation and differentiation
A, H9C2 cells were cultured with IGF-I 48 h in the absence or presence of 10% serum (FBS). Results from multiple experiments were pooled by expressing data as a percentage of controls for each time point. *B*, H9C2 cells were cultured in serum-free medium in the presence or absence of a range of myostatin (MSTN) concentrations. Cells were grown for 48 h before the total cell number was measured. Results from multiple experiments were pooled and data are expressed as a percentage of controls. *C*, H9C2 cells were cultured for 48 h with the indicated combinations and concentrations (nM) of myostatin, IGF-I or LR3 in serum free medium. *D*, H9C2 cells were cultured in the presence or absence of 11 nM MSTN and stimulated to differentiate in 1% FBS and 10 nM retinoic acid added daily. Equilibrative nucleoside transporter (ENT)-1 was used as a differentiation marker and was quantified using 'real-time' RT-PCR. (Myo, proliferating myoblasts; 3D/6D, days in differentiation medium; +, differentiation medium with 11 nM myostatin). Significant differences ($P \leq 0.05$) in each panel are indicated by different letters (comparisons within −/+ serum groups, not between groups in panel *A*) whereas groups sharing the same letters are not different.

Table 2. Cardiac performance of wild-type and myostatin null mice

Parameter	WT	WT + ISO	Null	Null + ISO
LVIDd	3.02 ± 0.14 a	2.52 ± 0.05 b	3.50 ± 0.09 c	2.93 ± 1.01 a
LVIDs	2.03 ± 0.11 a	1.17 ± 0.04 b	2.73 0.08 c	1.6 ± 0.01 d
IVSd	0.82 ± 0.02 a	0.88 ± 0.03 a	0.87 ± 0.03 a	0.95 ± 0.04 a
LVWd	0.87 ± 0.04 a	0.92 ± 0.04 a	0.88 ± 0.03 a	1.03 ± 0.03 b
Diast vol	0.07 ± 0.01 a	0.042 ± 0.001 b	0.110 ± 0.009 c	0.065 ± 0.006 a
Syst vol	0.022 ± 0.004 a	0.007 ± 0.001 b	0.053 ± 0.005 c	0.009 ± 0.001 b
FS	33.1 ± 1.0 a	53.6 ± 1.4 b	21.5 ± 2.5 c	46.75 ± 2.4 b
EF	68.8 ± 1.3 a	89.2 ± 0.9 b	49.3 ± 4.5 c	83.7 ± 2.1 b
Stroke vol	0.050 ± 0.006 a	0.037 ± 0.002 b	0.055 ± 0.008 a	0.055 ± 0.006 a
LV IVRT	23.0 ± 1.5 a	15.2 ± 1.0 b	24.8 ± 2.1 a	17.0 ± 0.8 b
Ao velo	83.3 ± 7.8 a	117.7 ± 11.0 b	103.2 ± 11.1 a	164.8 ± 12.6 c
Ao VTI	3.4 ± 0.5 a	5.2 ± 0.4 b	4.3 ± 0.4 a	6.3 ± 0.6 b
Ao acel	14.2 ± 1.7 a	5.8 ± 0.5 b	13.7 ± 1.9 a	10.2 ± 1.4 a
Ao ET	63.3 ± 3.4 a	69.2 ± 3.1 a	65.6 ± 3.5 a	62.8 ± 3.7 a
Ao ac/ET	0.24 ± 0.3 a	0.07 ± 0.1 b	0.21 ± 0.03 a	0.16 ± 0.02 a
MV E	84.7 ± 11.5 a	N.A.	92.3 ± 10.6	121 ± 8.1 ($n = 3$)
MV A	59.8 ± 4.9 a	147.8 ± 8.6 b	54.5 ± 8.1 a	136 ± 16.5 b
MV E/A	1.4 ± 0.2 a	N.A.	1.8 ± 0.2	1.2 ± 0.2 ($n = 3$)
MV DT	25.5 ± 1.8 a	N.A.	28.5 ± 1.5	26 ± 0.6 ($n = 3$)
LV mass	0.080 ± 0.005 a	—	0.106 ± 0.007	—
HR	361.5 ± 9.8 a	443.4 ± 18.4 b	346.7 ± 17.8 a	460.3 ± 16.8 b

WT, wild-type $mstn^{+/+}$ mice; null, $mstn^{-/-}$ mice; ISO, isoproterenol; LVIDd, left ventricle internal diameter (end diastole, mm); LVIDs, LVID systole; IVSd, intraventricular septum (dimension end diastole, mm); LVWd, LV wall dimension (systole, mm); Diast vol, LV end diastolic volume (ml); Syst vol, LV end systolic volume (ml); FS, % fractional shortening; EF, % ejection fraction; LV IVRT, LV isovolumic relaxation time (ms); Ao velo, max aortic ejection velocity (cm s^{-1}); VTI, velocity time intergral (cm); acel, ejection acceleration time (ms); ET, ejection time (ms); ac/ET, ratio of acel to ET; MV E, max LV early filling velocity (cm s^{-1}); A, max LV late filling (atrial contraction) velocity (cm s^{-1}); E/A, ratio of E to A velocities; DT, deceleration time of early LV filling (ms); LV mass, left ventricle mass (g); HR, heart rate (b m^{-1}); N.A., not available. Different letters denote statistical differences within each parameter, although not all parameters were assessed due to insufficient n.

null hearts, in both sexes, are heavier than WT hearts (Fig. S2). These differences are not readily distinguished until after 100 days unless HW is normalized to tail length, which unlike BW, does not differ between WT and null mice.

Resting fractional shortening (FS) and ejection fraction (EF) were significantly decreased, although stroke volume was similar in null and wild-type mice. Cardiac stress tests were therefore performed by administering isoproterenol (ISO), a β-adrenergic receptor agonist (Table 2 and Fig. 3*B*), to distinguish pathological from physiological hypertrophy (depressed *vs.* enhanced responsiveness, respectively). The percentage change in internal diameters and diastolic volume was similar in both groups despite absolute differences attributed to the eccentric hypertrophy in null mice (Table 2). However, the reduction in systolic volume was significantly greater (lower volumes at systole) in myostatin null mice and was accompanied by greater increases in fractional shortening and ejection fraction. As expected, ISO-induced tachycardia reduced stroke volume in wild-type mice, although by contrast, stroke volume actually increased in null mice. Thus, stress-induced relaxation and contractile capacity and cardiac output appear to have increased in null mice. The change in aortic acceleration (Ao acel) was greater in null mice and resulted in a shorter ejection time (Ao ET) and increased acel/ET ratio. The change in heart rate was also greater in null mice and may have contributed in part to the haemodynamic differences. The increased heart rate in response to ISO prevented comparisons of left ventricle filling parameters, which often occurs when performing stress tests on mice. These parameters, however, were distinguished in some or all of the null mice, contrary to wild-type mice (Table 2), and are possibly due to longer diastolic filling times in the null mice. Cardiac hypertrophy can result from physiological or pathological means (McMullen & Jennings, 2007; Catalucci *et al.* 2008) and the latter is associated with the upregulation of fetal cardiac genes (ANP, BNP, α-actin and b-MHC). However, these genes were normally expressed in myostatin null hearts (Fig. S3). Collectively, these results indicate that the eccentric hypertrophy that occurs in myostatin null hearts is physiological, not pathological.

Cardiac expression of myostatin and its binding proteins following an infarct

To help determine myostatin's role in regenerating cardiac muscle, the expression of myostatin, follistatin and FSTL-3 was measured in infarcted, border-infarcted and non-infarcted cardiac muscle 28 days after ischaemia–reperfusion injury. Normalized expression levels for all three genes were highly variable (Fig. S3), especially in the border-infarcted and infarcted muscle. Myostatin expression was therefore similar in the different regions. Despite this variability, expression of follistatin and FSTL-3 was highly elevated in the affected tissues, although these differences were only significant within the infarcted muscle.

Myostatin decreases excitation–contraction coupling in ventricular myocytes

Contractility and $[Ca^{2+}]_i$ were measured in wild-type and myostatin null ventricular myocytes as a means to investigate the mechanisms underlying the enhanced cardiac performance of myostatin null hearts. Field stimulations evoked larger $[Ca^{2+}]_i$ transients in ventricular myocytes from myostatin null mice than from wild-type. This occurred under control conditions and after the application of 100 nM ISO (Fig. 4). In fact, the control $[Ca^{2+}]_i$ transients of myostatin null cells were greater than the ISO-induced transients of wild-type cells. Furthermore, the overall ISO responsiveness (% increase w\ ISO) was also greater (Fig. 4*A*). These effects were likely to be due to larger SR Ca^{2+} loads in the null cells, as indicated by the amplitude of caffeine-induced $[Ca^{2+}]_i$ transients (Fig. 4*B*).

We also examined the dependence of cellular shortening (CS) on $[Ca^{2+}]_i$ during the contractile cycle *in vitro* (Fig. 5). As with $[Ca^{2+}]_i$ transients, both basal and ISO-stimulated CS were greater in myostatin null cells (Fig. 5*A* and *B*). Mapping the contractile cycle revealed a clear hysteresis relationship between CS and $[Ca^{2+}]_i$ in cells from both animals (Fig. 5*C*). Hysteresis is known to occur in WT cells (Esposito *et al.* 2000) and reflects the rapid release of Ca^{2+} by the EC coupling mechanism (Ca^{2+}-induced Ca^{2+} release) and the relatively slow responsiveness of the contractile machinery. Null cells had a larger hysteresis loop than wild-type cells (w\ or w\o ISO), suggesting similar, albeit enhanced, contractile kinetics. These differences were further examined by comparing peak shortening to peak $[Ca^{2+}]_i$ (Fig. 5*D*), which revealed identically steep relationships for

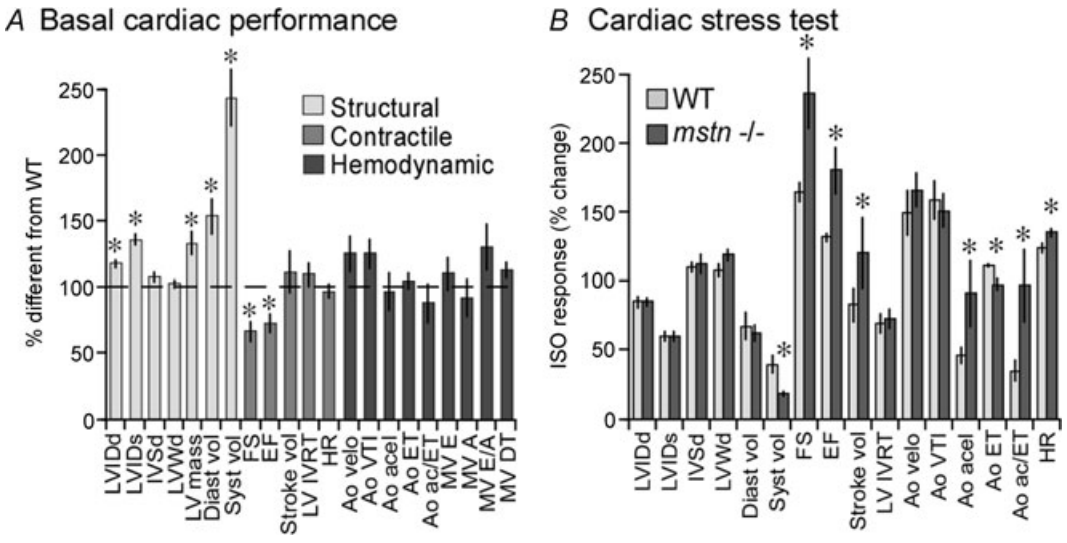

Figure 3. Enhanced resting and stress-induced cardiac performance in myostatin null mice
A, echocardiography was performed on the LV parasternal long axis, left parasternal short axis and subcostal long axis views. Data are presented as percentage difference from wild-type (WT) values represented by the horizontal dashed line (LVIDd, left ventricle internal diameter (end diastole, mm); LVIDs, LVID systole; IVSd, intraventricular septum (dimension end diastole, mm); LVWd, LV wall dimension (systole, mm); Diast vol, LV end diastolic volume (ml); Syst vol, LV end systolic volume (ml); FS, % fractional shortening; EF, % ejection fraction; LV IVRT, LV isovolumic relaxation time (ms); Ao velo, max aortic ejection velocity (cm s^{-1}); VTI, velocity time intergral (cm); acel, ejection acceleration time (ms); ET, ejection time (ms); ac/ET, ratio of acel to ET; MV E, max LV early filling velocity (cm s^{-1}); A, max LV late filling (atrial contraction) velocity (cm s^{-1}); E/A, ratio of E to A velocities; DT, deceleration time of early LV filling (ms); LV mass, left ventricle mass (g); HR, heart rate (b m^{-1}).) Structure, contractility and haemodynamic parameters are grouped and are indicated by differential shading. *B*, mice were injected intraperitoneally with 10 mg kg^{-1} ISO. Data are represented as percentage change from resting values (before ISO treatment). In both *A* and *B*, asterisks denote significant differences ($P \leq 0.05$, $n = 6$/group).

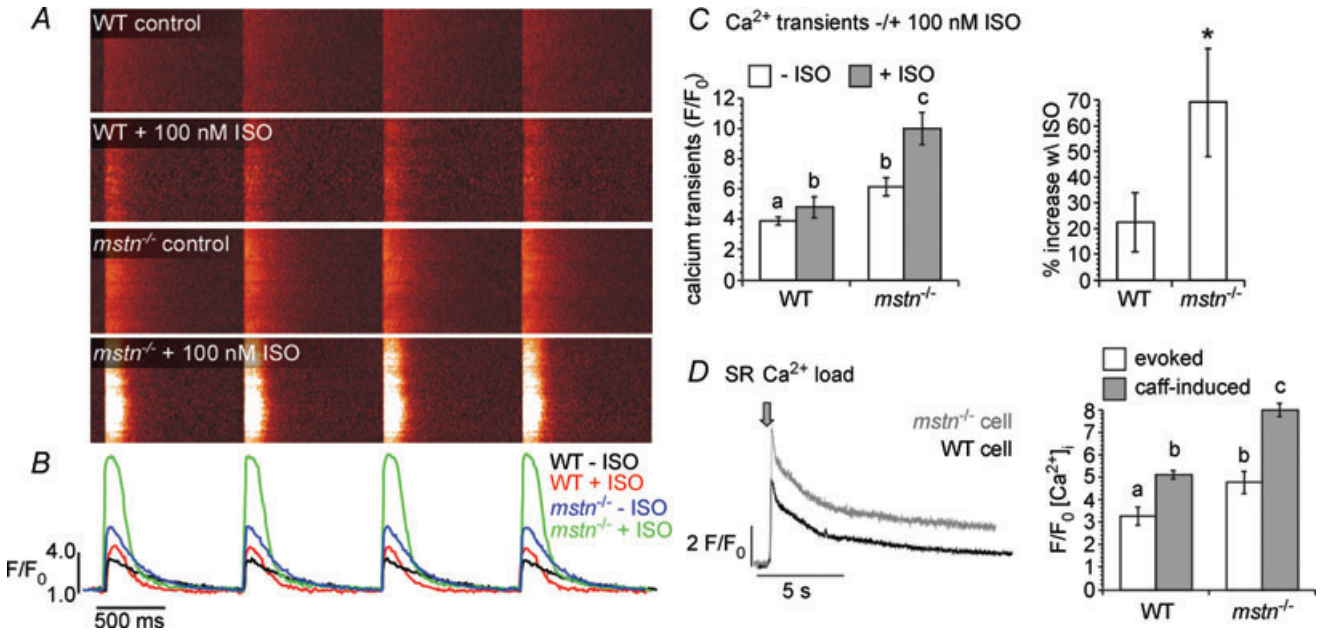

Figure 4. Myostatin decreases excitation–contraction coupling in ventricular myocytes
A, confocal line-scan images of evoked $[Ca^{2+}]_i$ transients (1 Hz) in WT and *mstn*−/− ventricular myocytes before and after the application of 100 nM ISO. *B*, the traces represent the spatially averaged time course of $[Ca^{2+}]_i$ in each of the images above. *C*, bar plots of $[Ca^{2+}]_i$ transient amplitudes before and after ISO (left) and percentage increase in $[Ca^{2+}]_i$ in response to ISO (right) in WT and *mstn*−/− myocytes. *D*, caffeine-induced $[Ca^{2+}]_i$ transients in typical WT and *mstn*−/− myocytes. The arrow marks the time when caffeine (20 mM) was applied. The bar plot shows the mean ± S.E.M. of the amplitude of the caffeine-induced $[Ca^{2+}]_i$ transients in WT and *mstn*−/− myocytes. Significant differences ($P \leq 0.05$) in all panels are indicated by different letters or an asterisk, whereas groups sharing the same letters are not different.

both wild-type and myostatin null cells and indicated that EC coupling in the latter cells is not only enhanced, but clearly not pathological. These data collectively suggest that the larger SR Ca^{2+} loads of myostatin null myocytes results in larger $[Ca^{2+}]_i$ transients that subsequently enhance basal and ISO-induced contractions.

Myofibre tension and ATPase activity

To investigate whether increased contractility, either in myostatin null hearts or cells, was due to altered sarcomeric structure and protein expression/modification, we measured myofilament Ca^{2+} sensitivity, Ca^{2+}-activated

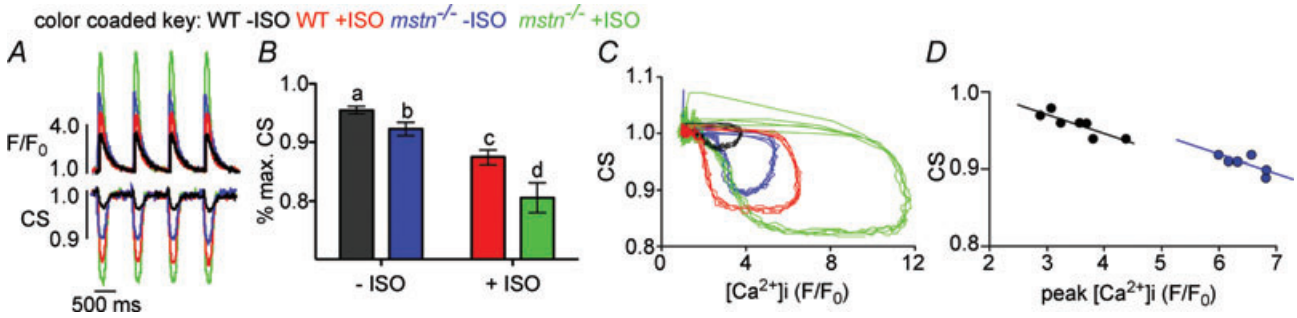

Figure 5. Myostatin decreases excitation–contraction coupling in ventricular myocytes
A, time course of $[Ca^{2+}]_i$ (top) and cell shortening (CS) in representative WT and *mstn*−/− ventricular myocytes before and after the application of 100 nM ISO. $[Ca^{2+}]_i$ transients were evoked via field stimulation (1 Hz). *B*, bar plot of the peak CS in WT and *mstn*−/− cells before and after ISO. Smaller values represent greater contractions and thus shorter cell lengths. Significant differences ($P \leq 0.05$) are indicated by different letters, whereas groups sharing the same letters are not different. *C*, relationship between $[Ca^{2+}]_i$ and CS, during four consecutive contractions, in WT and *mstn*−/− myocytes before and after ISO. Data are plotted as a trajectory. *D*, relationship between CS and $[Ca^{2+}]_i$ at peak $[Ca^{2+}]_i$ for ventricular myocytes taken from WT and *mstn*−/− animals. Data points were chosen to reflect the relationships shown in panel *C* as they arise vertically for a number of points at the maximal $[Ca^{2+}]_i$.

tension/ATPase activity and tension-dependent ATP consumption in detergent skinned muscle fibres. Normalized pCa–tension relations of all fibres were measured at a sarcomere length of 2.2 μm. The relationship between pCa and tension or ATPase activity was the same in fibres from wild-type and myostatin null hearts (Fig. 6*A*, *B* and *D*). Indeed, the pCa_{50} values (k) representing midpoints of both relationships and the maximum values for tension and ATPase activity were nearly identical in both groups. However, fibres from myostatin null hearts exhibited a slightly higher Hill coefficient (n), which is a measure of cooperativity for developing tension and ATPase activity (Fig. 6*D*). The tension–cost relation is a measure of the amount of ATP hydrolysed for a given amount of isometric tension produced and is influenced by changes in contractile protein expression, such as shifts in myosin heavy chain isoforms and/or thin filament regulatory proteins. Nevertheless, the relationships from both groups were similarly linear and the maximum values did not differ (Fig. 6*C* and *D*).

Discussion

Our study is the first to extensively assess myostatin's inhibitory effects on cardiac muscle growth and functional capacity. Most importantly, it is also the first to characterize what appears to be physiological hypertrophy in myostatin null mice. The lack of a well established cardiac phenotype among different myostatin null animals is somewhat surprising as several studies have implied functional roles for myostatin in the heart (Rodgers & Garikipati, 2008). Indeed, skeletal and cardiac muscle mass are both reduced in transgenic mice overexpressing myostatin (Reisz-Porszasz *et al.* 2003) and recent studies have clearly demonstrated myostatin's ability to inhibit some cardiac muscle growth processes (Morissette *et al.* 2006; Artaza *et al.* 2007; McKoy *et al.* 2007).

Both cardiac muscle and H9C2 cells express a complete complement of myostatin/activin receptors as well as two notable myostatin binding proteins, follistatin and FSTL-3 (Fig. 1). Thus, myostatin action in both muscle types is likely to be similarly regulated. Levels of Acvr2 expression were higher than those of Acvr2b in all the samples (Fig. 1), consistent with skeletal muscle expression (Lee *et al.* 2005), while the muscle mass of transgenic mice overexpressing dominant-negative Acvr2 is greater than that of mice overexpressing dominant-negative Acvr2b (Lee *et al.* 2005). This suggests that although myostatin is capable of signalling through both receptors, Acvr2 may play a more important role than previously presumed.

The pattern of myostatin expression in differentiating H9C2 cells (Fig. 1) is similar to that which occurs in developing fetal, neonatal and adult hearts (Poolman & Brooks, 1998; Sharma *et al.* 1999; McKoy *et al.* 2007). This further validates the H9C2 model and is consistent with myostatin's role as a cardiac muscle differentiation factor. Indeed, we corroborated previous results (Artaza *et al.* 2007; McKoy *et al.* 2007) demonstrating myostatin inhibition of basal cardiomyoblast proliferation (Figs 2 and 3). We also demonstrated, for the first time, that myostatin inhibits IGF-stimulated proliferation. These results together suggest that myostatin's inhibitory effects are fundamentally conserved in both muscle types.

Myostatin inhibits the proliferation of porcine embryonic myogenic cells in part by the local production of IGFBP-3 and -5 (Kamanga-Sollo *et al.* 2003, 2005; Pampusch *et al.* 2005; Xi *et al.* 2005), which sequester

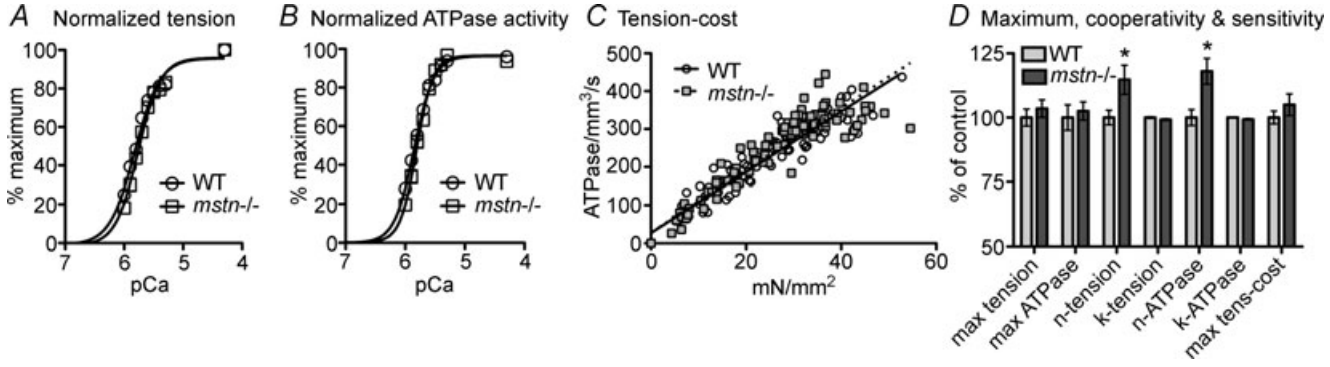

Figure 6. Biophysical assessment of skinned cardiac muscle from wild-type (WT) and myostatin null (*mstn*$^{-/-}$) mice

Resting sarcomere length was adjusted to 2.2 μm. *A*, normalized pCa–tension relation of skinned fibres from WT ($pCa_{50} = 5.79 \pm 0.02$, $n = 1.86 \pm 0.05$) and *mstn*$^{-/-}$ ($pCa_{50} = 5.74 \pm 0.02$, $n = 2.13 \pm 0.11$) hearts. *B*, normalized pCa–ATPase relation of fibres from WT ($pCa_{50} = 5.84 \pm 0.01$, $n = 2.44 \pm 0.11$) and *mstn*$^{-/-}$ ($pCa_{50} = 5.80 \pm 0.02$, $n = 2.98 \pm 0.13$) hearts. *C*, slopes of the tension–ATPase relations for WT and *mstn*$^{-/-}$ fibres (8.11 ± 0.2 and 8.51 ± 0.34 pmol mN^{-1} mm^{-1} s^{-1}, respectively). *D*, differences in the maximum (max), cooperativity (n) and sensitivity (k, pCa_{50}) values for tension, ATPase activity and tension-cost. Values are presented as means ± S.E.M. ($n = 10$, $P \leq 0.05$).

IGF-I outside the cell and may also inhibit the intracellular/nuclear actions required for growth (Oufattole *et al.* 2006; Xi *et al.* 2007). However, IGFBPs do not appear to mediate myostatin's actions in H9C2 cells as it suppressed the proliferative effects of IGF-I and LR3 equally (Fig. 2). Myostatin also suppresses IGF- and phenylephrine-stimulated protein synthesis in fully differentiated cardiomyocytes and directly inhibits cardiomyocyte size (Shyu *et al.* 2005; Morissette *et al.* 2006; McKoy *et al.* 2007). Its inhibitory effects on IGF action are, therefore, not limited to differentiation status. Our results also indicate that myostatin at least partially suppresses H9C2 cell differentiation (Fig. 2). These effects were lost by day 6, although myostatin was only added on days 1 and 3. Thus, the myokine's suppressive effects were likely to have been nullified in part by daily stimulation with retinoic acid. Similar studies with primary cells are needed to definitively determine myostatin's role during cardiomyoblast differentiation. Nevertheless, these results suggest that myostatin inhibits all of the processes required for the development of mature cardiac muscle: proliferation, differentiation and protein synthesis.

Previous studies have disagreed on the cardiac phenotype of myostatin null animals. Morissette *et al.* (2006) reported increased heart mass in female myostatin null mice and decreased mass in males, although these differences were not statistically significant. By contrast, Artaza *et al.* (2007) reported increases in heart mass and left ventricle size and Cohn *et al.* (2007) reported similar trends that were not statistically different. We therefore reexamined the cardiac phenotype using a much more extensive echocardiographic analysis than previously reported (21 *vs.* 5–7 parameters) and by physically weighing hearts from mice of various ages. Echocardiography was performed on resting hearts and for the first time on hearts stimulated with ISO (Table 2 and Fig. 3). The physical weighing of hearts and echocardiographical estimates both suggest that hearts from adult male and female myostatin null mice are larger than WT hearts. Differences in non-normalized heart weights were only distinguishable after 100 days (Fig. S2), which likely explains the discrepancies previously noted by Morissette *et al.* (2006) who used 56-day-old mice. The parallel increase in heart and body weights suggests that similar mechanisms may control both phenotypes. However, the many direct effects of myostatin on cardiac muscle cells suggest that cardiac hypertrophy is not a compensatory response to hypermuscularity. In fact, the increased musculature resulting from isometric exercise produces concentric hypertrophy (McMullen & Jennings, 2007; Catalucci *et al.* 2008) whereas myostatin null mice have eccentric hypertrophy. Neonatal heart and body weights of myostatin null pups were slightly less than those of wild-type (Fig. S1). Thus, cardiac hypertrophy in myostatin null mice develops postnatally or is at least an ontological consequence, but is not due entirely to enhanced development *in utero*.

The eccentric hypertrophy in myostatin null mice was accompanied by significantly lower systolic contraction functions at rest (FS and EF), similar stroke volumes and a heightened response to β-adrenergic stimulation. These results suggest that myostatin regulation of cardiac muscle development directly influences cardiac performance at rest and during a stress test. Cohn *et al.* (2007) used 24-month-old mice and Morissette *et al.* (2006) used non-anaesthetized mice. It is therefore difficult to determine whether age or handling stress was somehow a confounding factor. In fact, Cohn *et al.* (2007) reported identical body weights for both wild-type and myostatin null mice, which conflicts with the latter group's well documented double muscled phenotype (Rodgers & Garikipati, 2008). Morissette *et al.* (2006) also determined that myostatin inhibits the size of primary cardiomyocytes *in vitro*, which is consistent with the results presented herein and by Artaza *et al.* (2007).

Cardiac hypertrophy *per se* is not necessarily harmful as it can arise from either pathological or physiological means, of which the latter is unquestionably good. The two phenotypes are molecularly and functionally distinct as pathological hypertrophy is associated with contractility disorders and the expression of fetal genes (ANP, BNP, smooth muscle α-actin and β-MHC) while the opposite is true of physiological hypertrophy (McMullen & Jennings, 2007; Catalucci *et al.* 2008; Stout, 2008). Unlike cardiomyopathic hearts, the myostatin null hearts possessed an exaggerated β-adrenergic responsiveness (Fig. 3) and normal fetal cardiac gene expression profiles (Fig. S3), and do not develop the interstitial fibrosis (Cohn *et al.* 2007) that occurs with pathological hypertrophy. In fact, myostatin stimulates fibroblast proliferation *in vitro* and increases skeletal muscle fibrosis *in vivo* (Li *et al.* 2008). Some elite athletes (cyclists from the Tour de France and triathletes) who combine endurance and strength training possess functional cardiac profiles that are remarkably similar to those described of myostatin null mice (Claessens *et al.* 2000; Pluim *et al.* 2000; Whyte *et al.* 2000). This includes eccentric hypertrophy and reduced resting FS and EF values. These latter values rise to normal with detraining (Pavlik *et al.* 1986; Abergel *et al.* 2004) and are likely to be due to reduced preload in the presence of normal or enhanced afterload (Colan, 1992).

The cardiac stress tests revealed a heightened response to catecholamines in myostatin null mice as many cardiac systolic function and hemodynamic responses to ISO were proportionally greater in null than in wild-type mice (Fig. 3). This positively influenced cardiac performance, which is possibly best illustrated by the maintenance of stroke volume in null, but not wild-type mice. Thus, cardiac output was maintained in null mice despite the expected reduction in LV filling time

that occurs with increased heart rate. This heightened response was not simply due to physiological hypertrophy (i.e. larger, stronger hearts pumping more blood) as the ISO-stimulated heart rate was also faster in null mice. This suggests that myostatin and β-adrenergic signalling are at least acutely related. It also provides a potential mechanism by which myostatin may influence cardiac performance independent of its effects on growth. Indeed, basal and ISO-stimulated contractility and Ca^{2+} handling were both enhanced in primary ventricular myocytes from myostatin null hearts (Figs 4 and 5). The larger $[Ca^{2+}]_i$ transients (basal & stimulated) and SR load explain in part the increase β-adrenergic sensitivity while the similarly enhanced cellular shortening *in vitro*, again basal and ISO-stimulated, corroborate the echocardiographic results. The larger, yet normally shaped, hysteretic contractile cycle of myostatin null cells, as well as the identical relationships between peak shortening and peak $[Ca^{2+}]_i$ in both wild-type and null cells together indicate that the enhanced contractility of myostatin null hearts is replicated at the cellular level. Together, these results indicate that the myostatin null cardiac phenotype is clearly not pathological, although it resembles many elements of physiological hypertrophy seen in these highly trained athletes.

The myostatin null environment had no impact on most of the contractile functions tested in detergent-skinned cardiac muscle fibres. Thus, cardiomyocyte function is not altered at the myofilament level. It is difficult to ascertain the importance of the small, yet statistically significant increase in the Hill coefficient (Fig. 6*D*), which is a composite index of myofilament cooperativity that includes Ca^{2+} binding and near-neighbour interactions between regulatory subunits and cross-bridges (Gordon *et al.* 2000). Nevertheless, none of the other biophysical parameters differed between wild-type or myostatin null fibres, suggesting the slight increase in cooperativity did not influence overall myofilament function. More importantly, these data further indicate that the enhanced performance of myostatin null cardiomyocytes and hearts is due to Ca^{2+} handling and enhanced β-adrenergic signalling.

Skeletal muscle expression of myostatin mRNA and/or protein increases with various insults and contributes to the repair process by maintaining myosatellite cellular quiescence throughout the differentiation cycle (Rodgers & Garikipati, 2008). Its expression similarly increases in hypertrophied or infarcted cardiac muscle, although it is unknown whether the expression of myostatin binding proteins, which influence bioavailability, also change. Mean expression levels of follistatin and FSTL-3 were higher in the infarcted and border zones than in the non-infarcted zone (Fig. S3). The only statistically significant difference, however, occurred with follistatin. Myostatin expression was similar in all tissues, which was not necessarily surprising considering the large variability among samples. Whether or not these changes influence the development of pathological hypertrophy following an infarct remains to be determined. These results nevertheless suggest that regenerating cardiac muscle possesses the capacity to disrupt myostatin bioavailability through the local expression of myostatin binding proteins.

Disrupting myostatin bioactivity and/or availability may potentially impact the treatment of many clinical disorders. The data presented herein strongly suggest that targeting myostatin may help treat disorders of cardiac as well as skeletal muscle growth. Specifically, they suggest that myostatin blockade could help replace pathological hypertrophy of the heart with physiological hypertrophy and potentially improve clinical outcomes of patients recovering from a myocardial infarction. These therapeutics could also benefit cell-based procedures that depend upon the generation of viable cardiomyocytes from embryonic or non-embryonic stem cells (Laflamme *et al.* 2007; Nomura *et al.* 2007). Nevertheless, future studies with myostatin null mice will no doubt help determine the underlying mechanisms responsible for the development of physiological hypertrophy of the heart.

References

Abergel E, Chatellier G, Hagege AA, Oblak A, Linhart A, Ducardonnet A & Menard J (2004). Serial left ventricular adaptations in world-class professional cyclists: implications for disease screening and follow-up. *J Am Coll Cardiol* **44**, 144–149.

Adams GR (2002). Invited Review: Autocrine/paracrine IGF-I and skeletal muscle adaptation. *J Appl Physiol* **93**, 1159–1167.

Artaza JN, Reisz-Porszasz S, Dow JS, Kloner RA, Tsao J, Bhasin S & Gonzalez-Cadavid NF (2007). Alterations in myostatin expression are associated with changes in cardiac left ventricular mass but not ejection fraction in the mouse. *J Endocrinol* **194**, 63–76.

Catalucci D, Latronico MV, Ellingsen O & Condorelli G (2008). Physiological myocardial hypertrophy: how and why? *Front Biosci* **13**, 312–324.

Chandra M, Rundell VL, Tardiff JC, Leinwand LA, De Tombe PP & Solaro RJ (2001). Ca^{2+} activation of myofilaments from transgenic mouse hearts expressing R92Q mutant cardiac troponin T. *Am J Physiol Heart Circ Physiol* **280**, H705–713.

Chandra M, Tschirgi ML, Rajapakse I & Campbell KB (2006). Troponin T modulates sarcomere length-dependent recruitment of cross-bridges in cardiac muscle. *Biophys J* **90**, 2867–2876.

Claessens C, Claessens P, Claessens M & Claessens J (2000). Echocardiographic and physiological performance characteristics of triathletes. *Can J Cardiol* **16**, 993–1002.

Cohn RD, Liang HY, Shetty R, Abraham T & Wagner KR (2007). Myostatin does not regulate cardiac hypertrophy or fibrosis. *Neuromuscul Disord* **17**, 290–296.

Colan SD (1992). Mechanics of left ventricular systolic and diastolic function in physiologic hypertrophy of the athlete heart. *Cardiol Clin* **10**, 227–240.

Cook SA, Matsui T, Li L & Rosenzweig A (2002). Transcriptional effects of chronic Akt activation in the heart. *J Biol Chem* **277**, 22528–22533.

de Tombe PP & Stienen GJ (1995). Protein kinase A does not alter economy of force maintenance in skinned rat cardiac trabeculae. *Circ Res* **76**, 734–741.

Drummond AE, Le MT, Ethier JF, Dyson M & Findlay JK (2002). Expression and localization of activin receptors, Smads, and βglycan to the postnatal rat ovary. *Endocrinology* **143**, 1423–1433.

Esposito G, Santana LF, Dilly K, Cruz JD, Mao L, Lederer WJ & Rockman HA (2000). Cellular and functional defects in a mouse model of heart failure. *Am J Physiol Heart Circ Physiol* **279**, H3101–3112.

Farnworth PG, Wang Y, Leembruggen P, Ooi GT, Harrison C, Robertson DM & Findlay JK (2006). Rodent adrenocortical cells display high affinity binding sites and proteins for inhibin A, and express components required for autocrine signalling by activins and bone morphogenetic proteins. *J Endocrinol* **188**, 451–465.

Garikipati DK, Gahr SA, Roalson EH & Rodgers BD (2007). Characterization of rainbow trout myostatin-2 genes (rtMSTN-2a and -2b): Genomic organization, differential expression, and pseudogenization. *Endocrinology* **148**, 2106–2115.

Garikipati DK, Gahr SA & Rodgers BD (2006). Identification, characterization, and quantitative expression analysis of rainbow trout myostatin-1a and myostatin-1b genes. *J Endocrinol* **190**, 879–888.

Gaussin V & Depre C (2005). Myostatin, the cardiac chalone of insulin-like growth factor-1. *Cardiovasc Res* **68**, 347–349.

Gordon AM, Homsher E & Regnier M (2000). Regulation of contraction in striated muscle. *Physiol Rev* **80**, 853–924.

Helterline DL, Garikipati D, Stenkamp DL & Rodgers BD (2007). Embryonic and tissue-specific regulation of myostatin-1 and -2 gene expression in zebrafish. *Gen Comp Endocrinol* **151**, 90–97.

Kamanga-Sollo E, Pampusch MS, White ME & Dayton WR (2003). Role of insulin-like growth factor binding protein (IGFBP)-3 in TGF-β- and GDF-8 (myostatin)-induced suppression of proliferation in porcine embryonic myogenic cell cultures. *J Cell Physiol* **197**, 225–231.

Kamanga-Sollo E, Pampusch MS, White ME, Hathaway MR & Dayton WR (2005). Insulin-like growth factor binding protein (IGFBP)-3 and IGFBP-5 mediate TGF-β- and myostatin-induced suppression of proliferation in porcine embryonic myogenic cell cultures. *Exp Cell Res* **311**, 167–176.

Laflamme MA, Chen KY, Naumova AV, Muskheli V, Fugate JA, Dupras SK, Reinecke H, Xu C, Hassanipour M, Police S, O'Sullivan C, Collins L, Chen Y, Minami E, Gill EA, Ueno S, Yuan C, Gold J & Murry CE (2007). Cardiomyocytes derived from human embryonic stem cells in pro-survival factors enhance function of infarcted rat hearts. *Nat Biotechnol* **25**, 1015–1024.

Langley B, Thomas M, Bishop A, Sharma M, Gilmour S & Kambadur R (2002). Myostatin inhibits myoblast differentiation by down regulating MyoD expression. *J Biol Chem* **277**, 49831–49840.

Lee SJ, Reed LA, Davies MV, Girgenrath S, Goad ME, Tomkinson KN, Wright JF, Barker C, Ehrmantraut G, Holmstrom J, Trowell B, Gertz B, Jiang MS, Sebald SM, Matzuk M, Li E, Liang LF, Quattlebaum E, Stotish RL & Wolfman NM (2005). Regulation of muscle growth by multiple ligands signalling through activin type II receptors. *Proc Natl Acad Sci U S A* **102**, 18117–18122.

Leung GP, Tse CM & Man RY (2007). Characterization of adenosine transport in H9c2 cardiomyoblasts. *Int J Cardiol* **116**, 186–193.

Li ZB, Kollias HD & Wagner KR (2008). Myostatin directly regulates skeletal muscle fibrosis. *J Biol Chem* **283**, 19371–19378.

McKoy G, Bicknell KA, Patel K & Brooks G (2007). Developmental expression of myostatin in cardiomyocytes and its effect on foetal and neonatal rat cardiomyocyte proliferation. *Cardiovasc Res* **74**, 304–312.

McMullen JR & Jennings GL (2007). Differences between pathological and physiological cardiac hypertrophy: novel therapeutic strategies to treat heart failure. *Clin Exp Pharmacol Physiol* **34**, 255–262.

Menard C, Pupier S, Mornet D, Kitzmann M, Nargeot J & Lory P (1999). Modulation of L-type calcium channel expression during retinoic acid-induced differentiation of H9C2 cardiac cells. *J Biol Chem* **274**, 29063–29070.

Morissette MR, Cook SA, Foo S, McKoy G, Ashida N, Novikov M, Scherrer-Crosbie M, Li L, Matsui T, Brooks G & Rosenzweig A (2006). Myostatin regulates cardiomyocyte growth through modulation of Akt signalling. *Circ Res* **99**, 15–24.

Muller PY, Janovjak H, Miserez AR & Dobbie Z (2002). Processing of gene expression data generated by quantitative real-time RT-PCR. *Biotechniques* **32**, 1372–1374, 1376, 1378–1379.

Nomura T, Ashihara E, Tateishi K, Ueyama T, Takahas-Hi T, Yamagishi M, Kubo T, Yaku H, Matsubara H & Oh H (2007). Therapeutic potential of stem/progenitor cells in human skeletal muscle for cardiovascular regeneration. *Curr Stem Cell Res Ther* **2**, 293–300.

Oufattole M, Lin SW, Liu B, Mascarenhas D, Cohen P & Rodgers BD (2006). Ribonucleic acid polymerase II binding subunit 3 (Rpb3), a potential nuclear target of insulin-like growth factor binding protein-3. *Endocrinology* **147**, 2138–2146.

Pampusch MS, Xi G, Kamanga-Sollo E, Loseth KJ, Hathaway MR, Dayton WR & White ME (2005). Production of recombinant porcine IGF-binding protein-5 and its effect on proliferation of porcine embryonic myoblast cultures in the presence and absence of IGF-I and Long-R3-IGF-I. *J Endocrinol* **185**, 197–206.

Pavlik G, Bachl N, Wollein W, Langfy G & Prokop L (1986). Resting echocardiographic parameters after cessation of regular endurance training. *Int J Sports Med* **7**, 226–231.

Pluim BM, Zwinderman AH, Van Der Laarse A & Van Der Wall EE (2000). The athlete's heart. A meta-analysis of cardiac structure and function. *Circulation* **101**, 336–344.

Poolman RA & Brooks G (1998). Expressions and activities of cell cycle regulatory molecules during the transition from myocyte hyperplasia to hypertrophy. *J Mol Cell Cardiol* **30**, 2121–2135.

Reisz-Porszasz S, Bhasin S, Artaza JN, Shen R, Sinha-Hikim I, Hogue A, Fielder TJ & Gonzalez-Cadavid NF (2003). Lower skeletal muscle mass in male transgenic mice with muscle-specific overexpression of myostatin. *Am J Physiol Endocrinol Metab* **285**, E876–888.

Robey TE & Murry CE (2008). Absence of regeneration in the MRL/MpJ mouse heart following infarction or cryoinjury. *Cardiovasc Pathol* **17**, 6–13.

Rodgers BD & Garikipati DK (2008). Clinical, agricultural, and evolutionary biology of myostatin: a comparative review. *Endocr Rev* **29**, 513–534.

Santana LF, Chase EG, Votaw VS, Nelson MT & Greven R (2002). Functional coupling of calcineurin and protein kinase A in mouse ventricular myocytes. *J Physiol* **544**, 57–69.

Shao C, Liu M, Wu X & Ding F (2007). Time-dependent expression of myostatin RNA transcript and protein in gastrocnemius muscle of mice after sciatic nerve resection. *Microsurgery* **27**, 487–493.

Sharma M, Kambadur R, Matthews KG, Somers WG, Devlin GP, Conaglen JV, Fowke PJ & Bass JJ (1999). Myostatin, a transforming growth factor-β superfamily member, is expressed in heart muscle and is upregulated in cardiomyocytes after infarct. *J Cell Physiol* **180**, 1–9.

Shyu KG, Ko WH, Yang WS, Wang BW & Kuan P (2005). Insulin-like growth factor-1 mediates stretch-induced upregulation of myostatin expression in neonatal rat cardiomyocytes. *Cardiovasc Res* **68**, 405–414.

Stout M (2008). Athletes' heart and echocardiography: athletes' heart. *Echocardiography* **25**, 749–754.

Takehara-Kasamatsu Y, Tsuchida K, Nakatani M, Murakami T, Kurisaki A, Hashimoto O, Ohuchi H, Kurose H, Mori K, Kagami S, Noji S & Sugino H (2007). Characterization of follistatin-related gene as a negative regulatory factor for activin family members during mouse heart development. *J Med Invest* **54**, 276–288.

Van Den Berg G, Somi S, Buffing AA, Moorman AF & Van Den Hoff MJ (2007). Patterns of expression of the Follistatin and Follistatin-like1 genes during chicken heart development: a potential role in valvulogenesis and late heart muscle cell formation. *Anat Rec (Hoboken)* **290**, 783–787.

Whyte G, Lumley S, George K, Gates P, Sharma S, Prasad K & McKenna WJ (2000). Physiological profile and predictors of cycling performance in ultra-endurance triathletes. *J Sports Med Phys Fitness* **40**, 103–109.

Xi G, Hathaway MR, White ME & Dayton WR (2007). Localization of insulin-like growth factor (IGFBP)-3 in cultured porcine embryonic myogenic cells before and after TGF-β1 treatment. *Domest Anim Endocrinol* **33**, 422–429.

Xi G, Kamanga-Sollo E, Hathaway MR, Dayton WR & White ME (2005). Effect of constitutive expression of porcine IGFBP-3 on proliferation and differentiation of L6 myogenic cells. *Domest Anim Endocrinol* **31**, 35–51.

Author contributions

B.D.R. and L.F.S.: conception, design and performance of experiments, data analysis and interpretation, and manuscript writing; J.P.I., D.K.G., R.M. and O.L.N.: performance of experiments, data analysis and manuscript writing; M.C.: experimental design, data analysis and manuscript writing; C.E.M.; providing necessary reagents, data interpretation and manuscript writing. Approved by all authors.

Acknowledgements

This work was supported by grants from the National Institutes of Health (AR051917 to B.D.R., HL075643 to M.C., HL03174, HL64387, DK076126 and HL084642 to C.E.M. and HL085686 to L.F.S.). We thank Ms Sarah Dupras for performing the mouse myocardial infarcts and Mr Mark Saiget for isolating the mouse heart RNA. We are particularly grateful of Li Liang (MetaMorphix, Inc., Beltsville, MD, USA) for supplying the recombinant myostatin.